International Journal of Heat and Fluid Flow 30 (2009) 761–767

Contents lists available at ScienceDirect

International Journal of Heat and Fluid Flow

journal homepage: www.elsevier.com/locate/ijhff

A numerical investigation of electrohydrodynamic (EHD) effects on bubble deformation under pseudo-nucleate boiling conditions

Y.Q. Zu, Y.Y. Yan *

School of the Built Environment, University of Nottingham, Nottingham NG7 2RD, UK

ARTICLE INFO

Article history:
Received 19 June 2008
Received in revised form 23 December 2008
Accepted 23 March 2009
Available online 25 April 2009

Keywords:
EHD
Pseudo-nucleate boiling
Bubble deformation
CFD
VOF
Numerical modeling
Heat transfer

ABSTRACT

In this article, the electrohydrodynamic (EHD) effects on nucleate boiling are studied by developing a numerical modelling of EHD effect on bubble deformation in pseudo-nucleate boiling conditions. The volume of fluid (VOF) method is employed to track the interface between the gas–liquid two phases; the user-defined code is written and added to the commercial software FLUENT to solve the electric field and the corresponding electric body force. On this basis, the model is applied to study the EHD effects on heat transfer and fluid flows. An initial air bubble surrounded by liquid CCl_4 and attached to a horizontal superheated wall under the action of electric field is studied. The results of the EHD effect on bubble shape evolution are compared with those of available experiments showing good agreement. The mechanism of EHD enhancement of heat transfer and the EHD induced phenomena including bubble elongation and detachment are analyzed in detail.

1. Introduction

Nucleate boiling is an effective mode of heat transfer and it is very important for industrial processes because high heat transfer rates can be obtained despite relatively small temperature differences. Due to the benefits of high heat transfer rates and the demand of removal of large amounts of heat from small heated surfaces, which often occurs in the fast growing microchips industries, the enhancement of gas–liquid two-phase heat transfer has drawn researcher's particular attention for several decades and a number of effective techniques have been developed. Applying an electric field to a dielectric fluid to have an electrohydrodynamic (EHD) effect is an active technique for enhancing gas–liquid two-phase heat transfer in nucleate boiling and has demonstrated a great promise.

In the last few decades, many works on EHD enhancement of boiling heat transfer have been carried out; the attractiveness of the EHD technique has been increasingly recognized by the heat transfer society (Allen and Karayiannis 1995). In order to explain the mechanism of EHD-enhanced boiling heat transfer, much effort has been made to study the nucleate boiling of dielectric refrigerants in the presence of an electric field (Ogata and Yabe 1993a,b; Cho et al. 1996; Neve and Yan 1996; Cho et al. 1998; Karayiannis and Xu 1998a,b; Kweon et al. 1998; Di Marco et al. 2003; Madadnia and Koosha 2003; Dong et al. 2006; Chen et al. 2007; and more recently Pearson and Seyed-Yagoobi, 2008). Ogata and Yabe (1993a,b) carried out an experimental study and a basic numerical analysis of the EHD effect on nucleate bubbles; typically, in the numerical simulation (Ogata and Yabe, 1993b), the boundary condition of the electric field at the two-phase interface was defined as $\boldsymbol{n} \cdot \phi = 0$. Cho et al. (1996, 1998) performed numerical simulations and experiments to investigate the effect of uniform and non-uniform electric fields on a single bubble, respectively, and made the same assumption as Ogata and Yabe (1993a) did. However, as Karayiannis and Xu (1998a,b) pointed out, it is not reasonable to set the electric field strength **E** in the direction of normal to the sphere surface to be zero; an improved boundary condition was then applied. More recently, Pearson and Seyed-Yagoobi (2008), presented a three-dimensional mathematical model without requiring an axisymmetric configuration to simulate bubble deformation of dielectric fluid due to the presence of a nonuniform electric field and calculating the net dielectrophoretic force that is exerted by the electric field on the bubble. The reciprocal effect of the bubble's presence on the electric field is also incorporated into the model. The results indicate that the bubble deformation can be significant; bubble deformation and electric field distortion can have significant effects on the dielectrophoretic behaviour of bubbles in nonuniform fields, especially within small-scale devices where the bubble size and electrode spacing are similar in magnitude. On experimental visualisation, Madadnia and Koosha (2003) demonstrated the behaviours of isolated bubbles in pool nucleate

* Corresponding author. Tel.: +44 115 951 3168; fax: +44 115 951 3159.
E-mail address: yuying.yan@nottingham.ac.uk (Y.Y. Yan).

0142-727X/$ - see front matter © 2009 Elsevier Inc. All rights reserved.
doi:10.1016/j.ijheatfluidflow.2009.03.008

Nomenclature

c	specific heat
C	constant
D	diameter of the parallel plates
$\mathbf{E}$	electric field intensity
F	volume fraction
$\mathbf{F}_e$	electric body force
$\mathbf{g}$	gravitational acceleration
h	convective heat transfer coefficient
$\mathbf{I}$	identity tensor
k	turbulence kinetic energy
Nu	local Nusselt number
$\overline{Nu}$	surface averaged Nusselt number
S	source term
t	time
q	charge density
T	temperature
$\mathbf{u}$	velocity vector

Greek symbols

ε	turbulence dissipation rate (or permittivity of fluids)
ε_0	permittivity in space
ξ	user-defined scalar
λ	thermal conductivity
ρ	mass density
σ	surface tension
μ	dynamic viscosity
μ_t	turbulence viscosity
Γ	diffusion coefficient
ϕ	electric potential

Subscripts and superscripts

l	liquid phase
g	gas phase
T	transpose of tensor
k	turbulence kinetic energy
ε	turbulence dissipation rate
r	coordinate in radial direction
z	coordinate in axial direction

boiling in the presence of an electric field; and based on the visualisation, such parameters as bubble departure diameter, nucleation rate, and density of nucleation sites were studied. By applying a wire–wire electrode, a phenomenon that the bubble size was reduced by the imposing electric field was observed. Similar phenomenon has also been reported by Kweon et al. (1998). In general, the experiments have revealed that major effects of an electric field on nucleate boiling such as increasing bubble generating frequency, decreasing bubbles size, and increasing the maximum heat flux. However, to analyse the mechanism of EHD effects on nucleate boiling flow and heat transfer, the details of transport phenomena in the vicinity of gas–liquid interface of deformable bubbles should first be understood; and these have not been made clear so far by the experimental studies, because of the limitations of measurement methods. Although the numerical studies taking the advantages of increasing computational power could supply detailed information of interfacial flow for deformable bubbles, unfortunately, due to the complexity of the EHD nucleate boiling which is concerned with solving flow, temperature and electric fields simultaneously, the previous numerical studies are basically limited to model EHD affected bubbles without heat transfer or bubble deformation.

In the present study, a numerical model of EHD effect on nucleate boiling is developed based on the commercial code FLUENT; the volume of fluid (VOF) (Hirt and Nichols 1981) method is employed to track the interface between the gas–liquid two phases; the user-defined code is written and added to the software to solve the electric field and the corresponding electric body force. By solving the coupling problems of fluid flow, thermal and electric field, the effect of an applied electric field on heat transfer and flows for an air bubble surrounded by liquid CCl_4 and initially attached to a superheated horizontal wall are studied and simulated numerically. The numerical results are compared with available experimental data and the mechanism of EHD effects on heat transfer and bubble deformation of nucleate boiling are discussed.

2. Problem description

In order to study the mechanism of EHD effects on flow and heat transfer relevant to a nucleate bubble, an air bubble of diameter 0.2 mm surrounded by liquid CCl_4 and initially attached to the centre of an electrode as heated wall is considered; the contact angle of the bubble on the wall is of 60°; the corresponding geometry and initial and boundary conditions are as shown in Fig. 1. The electrodes are a pair of parallel round discs, with temperature difference ΔT and electric potential, $\Delta\varphi$; the lower disk is connected to the ground and is superheated during nucleate boiling. The diameter of the electrodes and the gap size between the electrodes are 1 mm. A no-slip boundary condition is specified at two disk; and a slip-free and insulated boundary (symmetry boundary) condition is given at $r = 0.5$ mm. The physical properties of liquid CCl_4 and air (Yao 1985; Zhang 2003) are shown in Table 1.

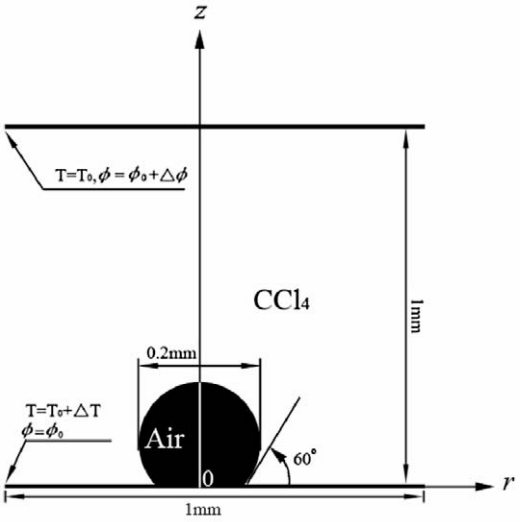

Fig. 1. Initial and boundary conditions.

3. Numerical methodology

3.1. The VOF method

For modelling two-phase flows, the VOF method (Hirt and Nichols 1981) is used to track a scalar field variable F, namely volume

Table 1
Physical properties of CCl_4 and air at 20 °C.

	CCl_4	Air
ρ	1584 kg m^{-3}	1.225 kg m^{-3}
μ	8.403×10^{-4} kg m^{-1} s^{-1}	1.7894×10^{-5} kg m^{-1} s^{-1}
λ	0.1055 Wm^{-1}K^{-1}	2.42×10^{-2} Wm^{-1} K^{-1}
c	4.182 kJ kg^{-1} K^{-1}	1.006 kJ kg^{-1} K^{-1}
ε	1.9822×10^{-11} Fm^{-1}	8.9385×10^{-12} Fm^{-1}
σ	2.643×10^{-2} Nm^{-1}	
ε_0	8.85×10^{-12} Fm^{-1}	

fraction, which stands for the distribution of the second fluid in the computational grid. As given in Eq. (1), F takes a value between 0 and 1 for the cell containing interface, and a value of 0 or 1 for the cell occupied by pure air or CCl_4, correspondingly.

3.1.1. Definition of F-function

$$\begin{cases} F = 0 & \cdots \text{ Air}, \\ 0 < F < 1 & \cdots \text{ Interface}, \\ F = 1 & \cdots \text{ } CCl_4. \end{cases} \tag{1}$$

In the VOF method, velocity field $\mathbf{u}$ and the distribution of volume fraction F are coupled to satisfy the following transport equation:

3.1.2. Transport equation of F

$$\frac{\partial F}{\partial t} + \nabla \cdot (\mathbf{u}F) = 0; \tag{2}$$

where t represents time. Eq. (2) must be solved together with the fundamental equations of conservation of mass, momentum and energy, to achieve computational coupling among the velocity field, temperature field and the phase distribution.

3.1.3. Equation of mass

$$\frac{\partial \rho}{\partial t} + \nabla \cdot (\rho \mathbf{u}) = 0. \tag{3}$$

3.1.4. Equation of momentum

$$\frac{\partial (\rho \mathbf{u})}{\partial t} + \nabla \cdot (\rho \mathbf{u}\mathbf{u}) = -\nabla p + \nabla \cdot [\mu(\nabla \mathbf{u} + (\nabla \mathbf{u})^{\mathrm{T}})] + \rho \mathbf{g} + \mathbf{F}_e. \tag{4}$$

3.1.5. Equation of energy

$$\frac{\partial}{\partial t}(\rho c T) + \nabla \cdot (\rho c \mathbf{u} T) = \nabla \cdot (\lambda \nabla T); \tag{5}$$

where c and λ are used to define specific heat and thermal conductivity of the fluids.

3.2. User-defined code for electric field

The electric body force in Eq. (4) can be given by the following equation (Stratton, 1941; Pollard et al. 2003):

$$F_e = q\mathbf{E} - \frac{1}{2}\mathbf{E}^2 \nabla \varepsilon + \frac{1}{2}\nabla \left[\mathbf{E}^2 \left(\frac{\partial \varepsilon}{\partial \rho} \right)_T \rho \right]. \tag{6}$$

Simply described, the three terms on the right-hand side of Eq. (6) represent the electrophoretic, dielectrophoretic, and electrostrictive components of the electric body force, respectively. The electrophoretic force (also known as the Coulomb force) results from the net free charge within the fluid or injected from the electrodes; The dielectrophoretic force is a consequence of inhomogeneity or spatial change in the permittivity of the dielectric fluid due to non-uniform electric fields, temperature gradients, and phase differences; The electrostrictive force is caused by inhomogeneous electric field strength and the variation in dielectric constant with temperature and density.Using the Clausius–Mossotti relationship (Lorentz 1952)

$$\frac{\varepsilon - \varepsilon_0}{\varepsilon + 2\varepsilon_0} = C\rho; \tag{7}$$

where C is constant, the electric body force can then be rewritten as

$$\mathbf{F}_e = q\mathbf{E} - \frac{1}{2}\mathbf{E}^2 \nabla \varepsilon + \frac{1}{6}\nabla \left[\mathbf{E}^2 \frac{(\varepsilon - \varepsilon_0)(\varepsilon + 2\varepsilon_0)}{\varepsilon_0} \right]; \tag{8}$$

where, q is the charge density, $\mathbf{E}$ the electric field intensity, ε the permittivity of fluids, and ε_0 the permittivity in space.

In the present simulation, only the electrostatic solution is used. Thus, q and $\mathbf{E}$ can be obtained by solve the following equation system:

$$\nabla \cdot (\varepsilon \nabla \phi) = 0; \tag{9}$$

$$\mathbf{E} = -\nabla \phi; \tag{10}$$

$$q = \varepsilon \nabla \cdot \mathbf{E}; \tag{11}$$

where ϕ is electric potential.

Unfortunately, the electric field can not be solved directly by FLUNENT software. Therefore, in the present study, a user-defined code is written to solve Eq. (9) and then the electric body force given by Eq. (8). For an arbitrary user-defined scalar ξ, FLUENT can solve the following transport equation (FLUENT, 2003):

$$\frac{\partial \rho \xi}{\partial t} + \nabla \cdot (\rho \mathbf{u} \xi - \Gamma \nabla \xi) = S; \tag{12}$$

where Γ and S are the diffusion coefficient and source term. For the steady-state case, if no convective flux and sour term are considered, i.e.

$$\frac{\partial \rho \xi}{\partial t} = 0; \tag{13a}$$

$$\nabla \cdot (\rho \mathbf{u} \xi) = 0; \tag{13b}$$

$$S = 0. \tag{13c}$$

Thus, Eq. (13c) can be simplified to the following form:

$$\nabla \cdot (\Gamma \nabla \xi) = 0. \tag{14}$$

The similarity of the Eqs. (9) and ((14)) yields that the quantities of the two equations have the following corresponding relationships:

$$\Gamma \Longleftrightarrow \varepsilon, \quad \xi \Longleftrightarrow \phi. \tag{15}$$

By substituting the above relevant parameter in Eq. (14), then the solver for Eq. (14) can also be used to solve Eq. (9).

The distribution of volume fraction has to be reconstructed at every time step. Meanwhile, the distribution of fluid properties is updated based on Eq. (16).

$$\begin{aligned} &\rho = \rho_l F + \rho_g (1 - F); \quad \mu = \mu_l F + \mu_g (1 - F); \quad \varepsilon = \varepsilon_l F + \varepsilon_g (1 - F) \\ &\lambda = \lambda_l F + \lambda_g (1 - F); \quad c = c_l F + c_g (1 - F). \end{aligned} \tag{16}$$

where the subscripts, l and g denote the values of liquid and gas phases, respectively.

3.3. Turbulent model

In the simulation, the standard $k - \varepsilon$ model (Launder and Spalding, 1972) is used to simulate the potential turbulence caused by bubble movement and EHD (Soldati, 2002); here, ε denotes the tur-

bulence dissipation rate rather than permittivity of fluids. The $k-\varepsilon$ model belongs to the Reynolds-averaged approach, in which the Reynolds-averaged Navier–Stokes (RANS) equations are used as the transport equations for the mean flow quantity; all of the scales of the turbulence are modelled based on certain assumptions. The RANS equation is written as:

$$\frac{\partial}{\partial t}(\rho\mathbf{u}) + \nabla\cdot(\rho\mathbf{u}\mathbf{u}) = -\nabla p + \nabla\cdot[\mu(\nabla\mathbf{u} + (\nabla\mathbf{u})^{\mathrm{T}})] + \rho\mathbf{g} + \mathbf{F}_e + \nabla\cdot(-\rho\overline{\mathbf{u}'\mathbf{u}'}). \quad (17)$$

Comparing the RANS momentum equation Eq. (17) with the Navier–Stokes momentum Eq. (4), the additional terms appear to represent the effect of turbulence. The Reynolds stresses, $-\rho\overline{\mathbf{u}'\mathbf{u}'}$, must be modelled in order to close Eq. (17). The $k-\varepsilon$ model employs the Boussinesq hypothesis (Hinze, 1975) to relate the Reynolds stresses to the mean flow velocity gradients:

$$-\rho\overline{\mathbf{u}'\mathbf{u}'} = \mu_t(\nabla\mathbf{u} + (\nabla\mathbf{u})^{\mathrm{T}}) - \frac{2}{3}(\rho k + \mu_t\nabla\cdot\mathbf{u})\mathbf{I}. \quad (18)$$

The turbulence kinetic energy, k, and its rate of dissipation, ε, are obtained from the following transport equations:

$$\frac{\partial}{\partial t}(\rho k) + \nabla\cdot(\rho k\mathbf{u}) = \nabla\cdot[(\mu + \mu_t/\eta_k)\nabla k] + G_k - \rho\varepsilon; \quad (19)$$

$$\frac{\partial}{\partial t}(\rho\varepsilon) + \nabla\cdot(\rho\varepsilon\mathbf{u}) = \nabla\cdot[(\mu + \mu_t/\eta_\varepsilon)\nabla\varepsilon] + +C_{1\varepsilon}\frac{\varepsilon}{k}G_k - C_{2\varepsilon}\rho\frac{\varepsilon^2}{k}; \quad (20)$$

where $C_{1\varepsilon}$ and $C_{2\varepsilon}$ are constants; η_k and η_ε are the turbulent Prandtl numbers for k and ε, respectively; G_k represents the generation of turbulence kinetic energy due to the mean velocity gradients and can be calculated by

$$G_k = -\rho\overline{\mathbf{u}'\mathbf{u}'} : (\nabla\mathbf{u}). \quad (21)$$

While the turbulent viscosity, μ_t, can be computed by combining k and ε as,

$$\mu_t = \rho C_\mu\frac{k^2}{\varepsilon}; \quad (22)$$

here C_μ is a constant. The default values of the model constants $C_{1\varepsilon}$, $C_{2\varepsilon}$, C_μ, η_k and η_ε are used:

$$C_{1\varepsilon} = 1.44, \quad C_{2\varepsilon} = 1.92, \quad C_\mu = 0.09, \quad \eta_k = 1.0, \quad \eta_\varepsilon = 1.3. \quad (23)$$

These default values have been found to work fairly well for a wide range of wall-bounded and free shear flows and therefore are used in the present simulation.

During the simulation, the implicit and unsteady solver is used for the solution of the system of governing equations. The momentum and energy equations are discretized using the second-order upwind scheme and the equation of volume fraction is discretized by Geo-Reconstruct scheme. The discretized equations are solved using the PISO algorithm. At each time step, the solution is assumed to be converged when the normalized residual of the energy equation is lower than 10^{-6} and the normalized residuals of continuity and other variables are less than 10^{-3}.

4. Results and discussion

For the current study, due to the symmetry of the problem, an axial symmetric coordinate system is used for the simulation. Electric potentials of 0, 15 and 30 kV are applied, respectively in the modelling. The corresponding evolutions of flow fields and temperature fields, when the time increases from 0 to 15 ms, are simulated. As shown in Fig. 2, 118×405 non-uniform rectangular

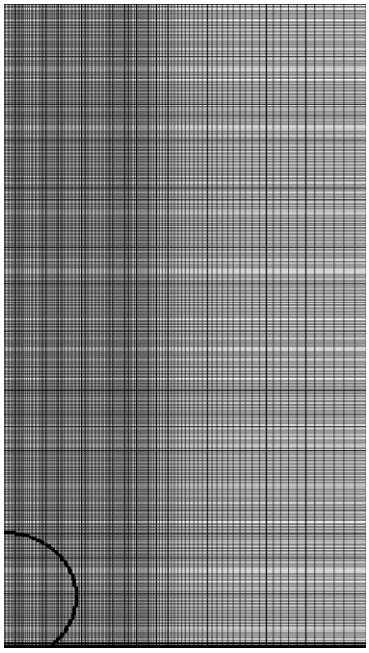

Fig. 2. Computational domain and meshes.

elements are used for meshing the computational domain, where the curved line shows the initial location of the interface between two fluids. Initial bubble radius occupies 40 grid points. Mesh near the lower boundary is fined to obtain the accurate velocity and thermal boundary layers. A grid sensitivity study is firstly performed on the basis of simulation for case when electric potential is 15 kV. It is found that the obtained local heat transfer coefficient on the heated wall and the local velocity at $r = 0$ change less then 0.08% and 0.1% respectively when the gird is doubly fined from 118×405 to 236×910 .

Fig. 3 shows the effects of electric field on bubble shapes. From the figure, it can be found that bubble is elongated by the electric field. Moreover, the period of the detachment increases with the voltage between the two parallel plates (the electrodes).

To validate the present model for flow field, the bubble shapes before the detachment from the heated wall at the voltage of 0, 15 and 30 kV, respectively, are compared with the experiments (Dong et al. 2006). Although the period of the bubble detachment can not be validated quantitatively as in Dong et al.'s experiment, an air bubble was injected through an orifice into the liquid CCl_4, Fig. 4 shows a comparison of the bubble shapes obtained by the present numerical simulation with those by experiments. Good agreement appears.

Fig. 5 shows the evolution of the distribution of dimensionless electric potential when the voltage between two parallel plates is 15 kV. The results indicate that the distribution of the electric field depends on the shape and position of the bubble and obviously. Moreover, unlike that in single phase flow, the distribution of the electric potential is not uniform due to the appearance of the bubble and non-uniform distribution of the permittivity.

To further check the mechanism of bubble elongation under the action of an electric field, the distribution of electric force over the air–CCl_4 interface at $t = 12.5$ ms and voltage 15 kV is calculated and the result is shown in Fig. 6. It can be seen that the bubble is pulled in axial direction and pushed in the negative radial direction by the electric body force, which results in the bubble elongation in the axial direction.

The effects of EHD on the heat transfer are studied from calculating the temperature field. As shown in Fig. 7, the variations with

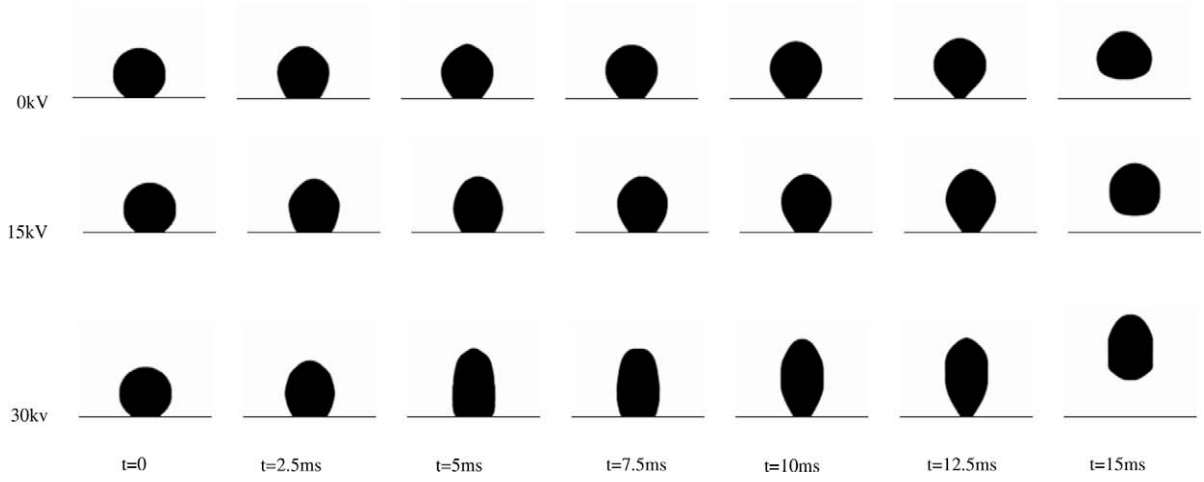

Fig. 3. Evolution of bubble shapes.

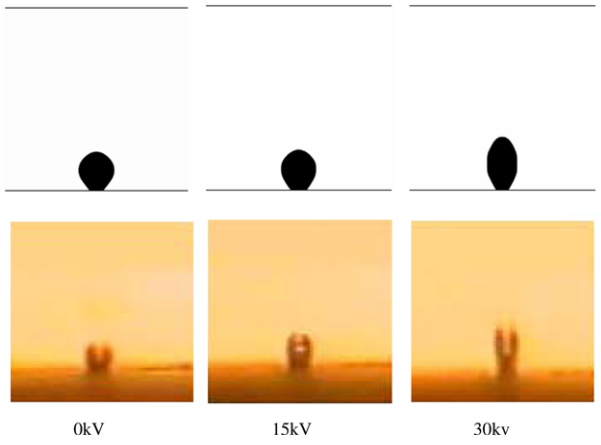

Fig. 4. Comparison of numerical results with experiments. (Top: obtained by present simulation; Bottom: obtained by experiments).

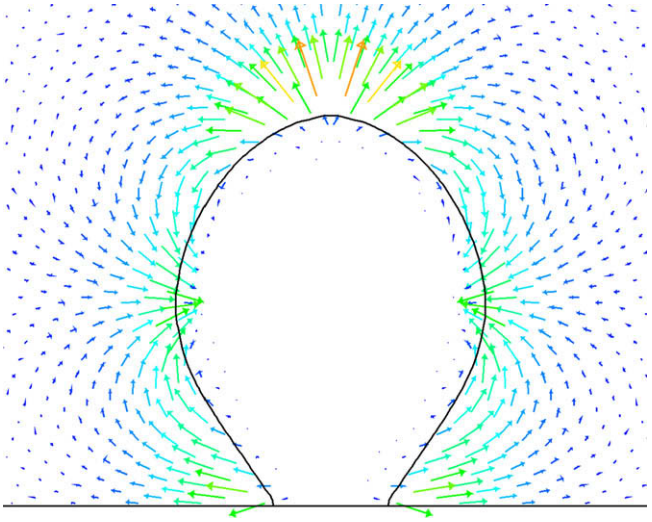

Fig. 6. Distribution of electric force ($\Delta\phi$ = 15 kV, t = 12.5 ms).

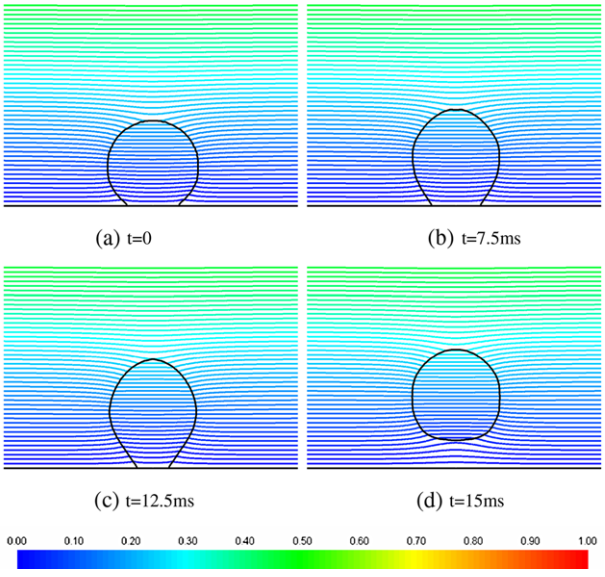

Fig. 5. Distribution of dimensionless electric potential ($\Delta\phi$ = 15 kV).

time of temperature fields over the gas–liquid interface at voltage of 0, 15 and 30 kV, respectively, are presented. It is obvious that the temperature distribution over the air–CCl_4 interface is very complex due to bubble shape and EHD induced local turbulence which enhances heat transfer.

In order to study the EHD effect on heat transfer efficiency, the following local and surface averaged Nusselt numbers, Nu and $\overline{Nu}$, are introduced:

$$Nu = \frac{hD}{\lambda_l}; \tag{24}$$

$$\overline{Nu} = \frac{2}{D}\int_0^{D/2} Nu(r)dr; \tag{25}$$

where h is heat transfer coefficient, r the radial coordinate, and D the diameter of the parallel plate.

Fig. 8 shows the distributions of the local Nusselt number on the heated wall at t = 12.5 ms and the voltages at 0, 15 and 30 kV, respectively. It can be noted that the local Nusselt number near the z-axis increases with the voltage. While, as shown in Fig. 9 which shows the variation with voltage of surface averaged Nusselt number on the heated wall, the averaged Nusselt number

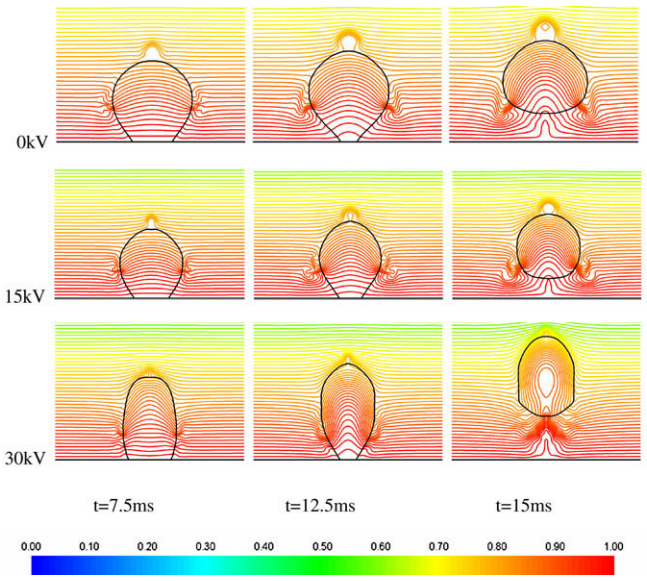

Fig. 7. Evolution of dimensionless temperature field ($\Delta\phi$ = 0 kV, 15 kV and 30 kV).

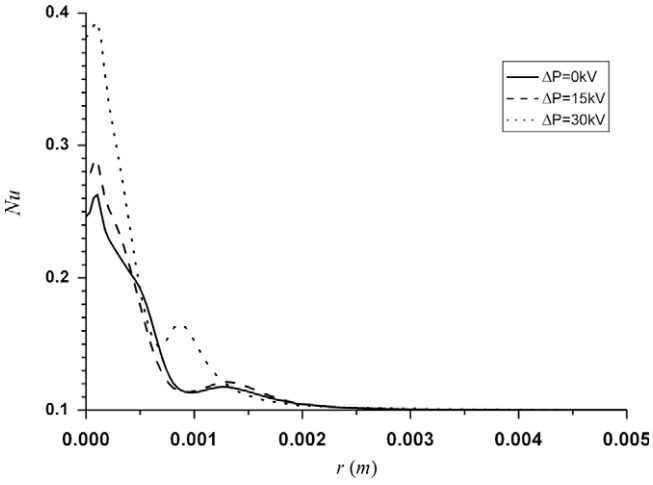

Fig. 8. Distribution of local Nusselt number on the heated wall (t = 12.5 ms).

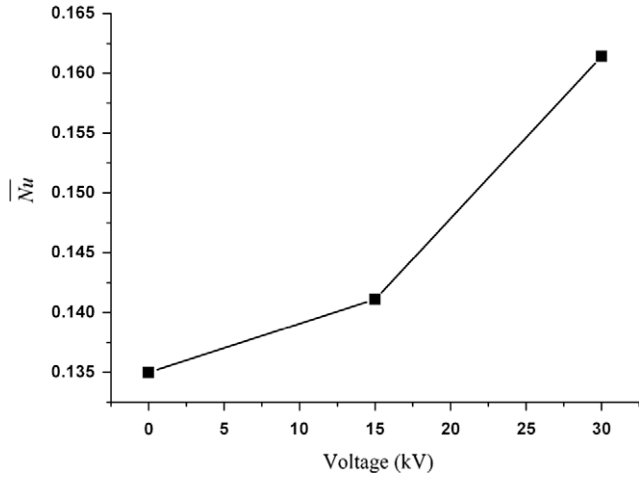

Fig. 9. Variation with voltage of surface averaged Nusselt number on the heated wall (t = 12.5 ms).

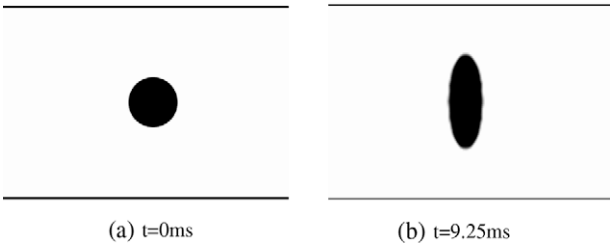

Fig. 10. Bubble deformation ($\Delta\phi$ = 30 kV).

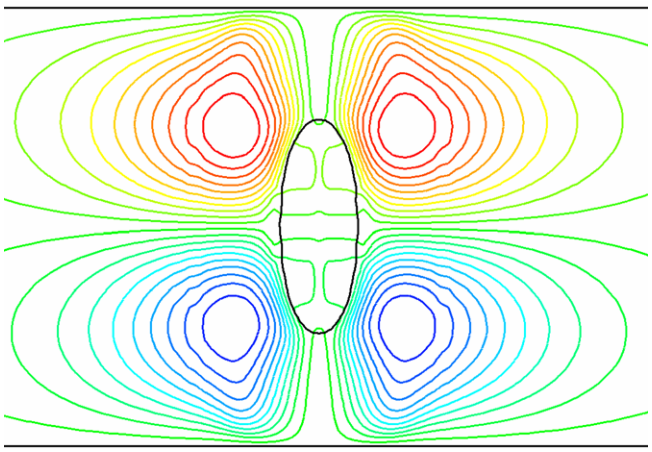

Fig. 11. Streamlines ($\Delta\phi$ = 30 kV).

increases with the voltage and meanwhile the corresponding increasing rate grows.

However, it should be pointed out that the mechanism of heat transfer enhancement by EHD cannot be easily analyzed from Fig. 7 because those temperature distributions are the results of the interaction of EHD, buoyancy force and wall adhesion. In order to find the mechanism of EHD enhancement on heat transfer, a specific case without the actions of buoyancy force and liquid–wall interactions is considered. As shown in Fig. 10, initially, a spherical bubble of diameter 0.2 mm is located at the centre of the computational domain with a uniform zero velocity; the voltage between two parallel plates is 30 kV. With the development of time, the bubble is deformed by only the electric field. Fig. 11 shows the streamlines at t = 9.25 ms. It indicates that ring vortices are induced by the electric field and therefore the shear-flow layer in the vicinity of liquid–bubble interface and the walls are formed; this type of vortices and shear flow result in the enhancement of heat transfer.

5. Conclusion

Numerical modelling of EHD effects on bubble deformation under pseudo-nucleate boiling conditions has been developed; the volume of fluid (VOF) method is employed to track the interface between bubble–liquid two phases; a user-defined code is written and added to the commercial CFD software to solve the electric field and the corresponding electric body force. The heat transfer and fluid flows when an air bubble surrounded by liquid CCl_4 and initially attached to a superheated horizontal wall with an electric field applied are studied and simulated numerically. The results of flow field agree well with those of previous experiments showing that the present method is suitable and can achieve accurate results of the EHD effects.

Meanwhile, through the numerical modelling and simulation, the mechanism of EHD effects on bubble shapes and heat transfer enhancement is studied and analyzed. The modelling shows that bubble is pulled in axial direction and pushed in the negative radial direction by the electric body force, which results in the bubble elongation in the axial direction. Moreover, the simulations also indicate that applying an electric field to nucleate boiling can enhance the motion of the vortices around the bubble and the walls as the thermal and fluid flows are seriously influenced by the electric body force; such vortex can enhance the heat transfer at the walls and gas–liquid interface.

References

Allen, P.H.G., Karayiannis, T.G., 1995. Electrohydrodynamic enhancement of heat transfer and fluid flow. Heat Recovery Systems and CHP 15 (5), 389–423.

Chen, F., Peng, Y., Song, Y.Z., Chen, M., 2007. EHD behavior of nitrogen bubbles in DC electric fields. Experimental Thermal and Fluid Science 32 (1), 174–181.

Cho, H.J., Kang, I.S., Kweon, Y.C., Kim, M.H., 1998. Numerical study of the behavior of a bubble attached to a tip in a nonuniform electric field. International Journal of Multiphase Flow 24 (3), 479–498.

Cho, H.J., Kang, I.S., Kweon, Y.C., Kim, M.H., 1996. Study of the behavior of a bubble attached to a wall in a uniform electric field. International Journal of Multiphase Flow 22 (5), 909–922.

Di Marco, P., Grassi, W., Memoli, G., Takamasa, T., Tomiyama, A., Hosokawa, S., 2003. Influence of electric field on single gas-bubble growth and detachment in microgravity. International Journal of Multiphase Flow 29 (4), 559–578.

Dong, W., Li, R.Y., Yu, H.L., Yan, Y.Y., 2006. An investigation of behaviors of a single bubble in a uniform electric field. Experimental Thermal and Fluid Science 30 (6), 579–586.

FLUENT, User's Guide. Fluent Inc, 2003.

Hinze, J.O., 1975. Turbulence. McGraw-Hill, New York.

Hirt, C.W., Nichols, B.D., 1981. Volume of fluid (VOF) method for the dynamics of free boundaries. Journal of Computational Physics 39 (1), 201–225.

Karayiannis, T.G., Xu, Y., 1998a. Electric field effect in boiling heat transfer part A: simulation of the electric field and electric forces. Journal of Enhanced Heat Transfer 5 (4), 217–229.

Karayiannis, T.G., Xu, Y., 1998b. Electric field effect in boiling heat transfer part B: electrode geometry. Journal of Enhanced Heat Transfer 5 (4), 231–247.

Kweon, Y.C., Kim, M.H., Cho, H.J., Kang, I.S., 1998. Study on the deformation and departure of a bubble attached to a wall in DC/AC electric fields. International Journal of Multiphase Flow 24 (1), 145–162.

Launder, B.E., Spalding, D.B., 1972. Lectures in Mathematical Models of Turbulence. Academic Press, London, England.

Lorentz, H.A., 1952. The Theory of Electrons. Dover, New York.

Madadnia, J., Koosha, H., 2003. Electrohydrodynamic effects on characteristic of isolated bubbles in the nucleate pool boiling regime. Experimental Thermal and Fluid Science 27 (2), 145–150.

Neve, R.S., Yan, Y.Y., 1996. Enhancement of heat exchanger performance using combined electrohydrodynamic and passive methods. International Journal of Heat and Fluid Flow 17 (4), 403–409.

Ogata, J., Yabe, A., 1993a. Augmentation of boiling heat transfer by utilizing the EHD effect – EHD behavior of boiling bubbles and heat transfer characteristics. International Journal of Heat and Mass Transfer 36 (3), 783–791.

Ogata, J., Yabe, A., 1993b. Basic study on the enhancement of nucleate boiling heat transfer by applying electric fields. International Journal of Heat and Mass Transfer 36 (3), 775–782.

Pearson, M.R., Seyed-Yagoobi, J., 2008. Numerical study of dielectric fluid bubble behavior within diverging external electric fields. Journal of Heat Transfer – Transactions of the ASME 130 (3). 1-10/032901.

Pollard, T.S., Cotton, J.S., Brocilo, D., Chang, J.S., Shoukri, M., 2003. Numerical simulation of electric field distributions in electrohydrodynamic two-phase flow regimes. IEEE Transactions on Dielectrics and Electrical Insulation 10 (1), 37–51.

Soldati, A., 2002. Influence of large-scale streamwise vortical EHD flows on wall turbulence. International Journal of Heat and Fluid Flow 23 (4), 441–443.

Stratton, J.A., 1941. Electromagnetic Theory. McGraw-Hill, New York.

Yao, Y.B., 1985. Handbook of Physics and Chemistry 5. Shanghai Science and Technology Press, Shanghai, China. pp. 234–237.

Zhang, H.L., 2003. Viscosity and density for binary mixtures of carbon tetrachloride plus chloroform, carbon tetrachloride plus dichloromethane, and chloroform plus dichloromethane and one ternary mixture of chloroform+1:1 (carbon tetrachloride plus dichloromethane) at 303.15 K. Journal of Chemical and Engineering Data 48 (1), 52–55.